Solid Inclusion Piezothermometry II: Geometric Basis, Calibration for the Association Quartz—Garnet, and Application to Some Pelitic Schists

HERBERT G. ADAMS[1,2]

Department of Geology, University of California,
Los Angeles, California 90024

LEWIS H. COHEN[2]

Department of Earth Sciences, University of California,
Riverside, California 92502

JOHN L. ROSENFELD[2]

Department of Geology, University of California,
Los Angeles, California 90024

Abstract

A procedure that enables determination of a pressure-temperature curve containing the pressure and temperature of incorporation of one mineral into a crystallizing host mineral consists of two steps. One step is determination of any experimentally-determined pressure and temperature for which a piezobirefringent halo in the host around the inclusion just vanishes. The second step uses a set of pressure-temperature curves, each of which indicates constant difference in natural strain between the two minerals as obtained by comparison dilatometry (Part I of this series). Barring complications, especially plastic creep, the curve that passes through the pressure and temperature at which the halo vanishes contains the pressure and temperature of incorporation. The intersection of two independently-determined curves of this type is the pressure and temperature of incorporation.

We report calibration of the association, quartz in three different orientations and garnet having a variety of compositions, to 7 kbar between 25°C and just below the low-high quartz transition. Extreme compositional variation within the solid solution $(Fe^{2+}, Mg, Ca, Mn^{2+})_3Al_2Si_3O_{12}$ has little effect on calibration. An implication of our work is that the linear coefficient of thermal expansion of almandine-type garnet near standard conditions is $\sim 7.58 \times 10^{-6} \, °C^{-1}$, considerably higher than previously accepted.

Tight pressure-temperature restrictions on the Al_2SiO_5 triple point, consistent with the determinations of Newton and of Holdaway, result from applications of solid inclusion piezothermometry and other petrological information to occurrences in New England and an Alpine occurrence. The inferred denudation rate of 0.5 ± 0.1 mm/year at the Alpine occurrence lies within the range of values obtained by Clark and Jäger from data on heat flow and geochronology at the nearly Gotthard Tunnel.

Introduction

Some years ago Rosenfeld and Chase (1961, p. 528–535) and Rosenfeld (1969, p. 320–331, 345–347) discussed application of comparison dilatometry to solid inclusion piezothermometry, a procedure for determination of the pressure and temperature at which a mineral inclusion was incorporated into a host mineral. In the previous paper of this series (Adams, Cohen, and Rosenfeld, 1975; hereafter referred to as Part I), we have detailed techniques of comparison dilatometry that were petrologically motivated.

In this paper we pursue further petrological goals by (1) elaboration of the general qualitative

---

[1] Present address: Department of Geology, California State University, Northridge, California 91324.
[2] The authors consider themselves equal partners in carrying out the work described herein.

geometric basis for solid inclusion piezothermometry, previously treated extensively and quantitatively for the special case of the host-inclusion pair, almandine-quartz (Rosenfeld, 1969, p. 320–328); (2) presentation of results of comparison dilatometry between garnet of various compositions and quartz in three orientations, extending the work of Adams *et al* (1970) to higher pressures; (3) correction, based upon experiments, of precalibration petrological inferences of Rosenfeld (1969, p. 335–345); and (4) addition of new observations on metamorphic rocks in western New England and the central Alps. We also briefly call attention to the discordance of our comparison dilatometry with previous X-ray diffraction work on synthetic almandine (Skinner, 1956).

Basis for Solid Inclusion Piezothermometry

Relationship of Geometry to Method

Assumptions of our model are that: (1) at the condition of envelopment (designated by subscript f) by the host, the inclusion is

(a) congruent to its cavity in the host;

(b) at the same temperature (T_f) as that of the host;

(c) at the same pressure (P_f) as that of the host; and that pressure is, for all practical purposes, hydrostatic;

and (2) after envelopment,

(d) host and inclusion are of such strength and stability that, within the lifetime of the combination and the conditions affecting it, all strains are solely elastic and thus not the consequence of plastic flow, phase transition, or radioactive damage;

(e) no tensile stress is maintainable across the interface between inclusion and host; and

(f) the inclusion does not shift irreversibly to a new position in the cavity.

The outline of the inclusion at P_f and T_f is the reference state for subsequently developed strains of inclusion and host.

For the purposes of analysis of ensuing strains and their implications, conceive the inclusion to be removed from the host without rotation and its outline to be superposed on the outline of the cavity in the host. Further, let host and inclusion, considered in this way, undergo identical changes in homogeneously distributed temperature and hydrostatic pressure.

If this assemblage, as imagined above, is subjected to a sufficiently wide range of pressure-temperature conditions, two regions in *P-T* space will logically arise if host and inclusion have different equations of state. Region *I* will be characterized by the presence of at least one direction in the inclusion for which its strain (≡ fractional change in length) is greater than the strain of the cavity in the same direction. Region *II* will be characterized by the absence of any direction for which the strain of the inclusion is as great as that of the cavity in the same direction. These two regions will be separated by a boundary along which, at each point, (1) there will be at least one direction in the inclusion for which the strain in the inclusion is equal to that in the host in the same direction; and (2) there will be no other direction for which the strain in the inclusion exceeds that of the host. That boundary will, of course, include P_f and T_f if the stated restrictions apply.

Now consider the inclusion within the host. By some procedure, permit access of a pressure medium of low viscosity to the host-inclusion interface. There will be a region of the *P-T* diagram within which the strains of both inclusion and host are governed by the second-rank tensor properties, thermal expansion and compressibility, which relate strain to the scalars, respectively temperature and hydrostatic pressure (Nye, 1957, p. 290). This region is characterized by those conditions for which all strains in the inclusion are less than those in the host in the same directions (*i.e.*, region *II*). This would not necessarily have been so if the pressure medium had not been permitted access to the host-inclusion interface.[3] Within region *I*, on the contrary, the situation is more complicated. There the strains of both inclusion and adjacent host are governed by second-rank thermal expansion tensors and fourth-rank compliance tensors, relating strain to nonhydrostatic stress. Accommodation of an inclusion, which in the model has at least one direction in which strain of the inclusion exceeds that of the host in the same direction, results in a halo of inhomogeneously distributed nonhydrostatic stress in the host around the inclusion.

In the absence of relaxational phenomena within or around the *in situ* inclusion, the boundary between regions *I* and *II* must pass through P_f and T_f. Further, *that boundary can be located because nonhydrostatic stress in the host around the inclusion in*

---

[3] The preceding sentences of this paragraph state the essential "trick" that allows avoidance of difficult problems in elasticity and permits use of hydrostatic pressure apparatus in our system of piezothermometry.

region I causes a stress-optical effect that is visible under the petrographic microscope. If a polished thick or thin section of the assemblage is made parallel to a section of zero birefringence in the host away from the influence of the inclusion, this effect, due to a field of deviatoric stress, expresses itself between crossed polars as a piezobirefringent halo. The boundary is then recognizable as the limiting *P-T* line for disappearance of the piezobirefringent halo.

Although it is more nearly precise to consider the assemblage in three dimensions, it is also useful in many cases to reduce the conceptual model to one that is approximately two dimensional rather than three dimensional (Rosenfeld, 1969, p. 318–329, 338). This particularly applies to thin sections in which a host-inclusion combination is cut so thin and in such an orientation as to have the cavity boundary penetrate the section essentially perpendicularly. The same analysis as in the previous paragraph applies, except that only strains parallel to the section are considered. The comparable subdivisions of the *P-T* diagram in this case will, in general, be different from that for the three-dimensional case except for highly symmetric combinations in which both host and inclusion are cubic. The boundaries, in either case, include P_f and T_f.

The principal advantages of the two-dimensional simplification over the three-dimensional approach are: (1) ease of laboratory observation: thin sections readily permit laboratory identification of conditions of equal strains in host and inclusion; (2) the fact that the direction of equal strains is very nearly restricted to the plane of the section; (3) the fact that sectioning permits access of a fluid medium of low viscosity and thus the operating pressure of the system to the region between host and inclusion;[4] and (4) the fact that the piezobirefringent halo becomes sensitive not only to *P* and *T* but also to the angular relations among the host, inclusion, and thin section.[5]

As defined in Part I, an *isomeke* is any *P-T* curve along which the distance between two reference points embedded in the hydrostatically stressed host mineral remains equal to that between two reference points embedded in the hydrostatically stressed inclusion mineral. The boundary between regions *I* and *II*, mentioned above, is an isomeke.

Determination of any isomeke, passing through P_f, T_f, is a two-step procedure. First, a comparison dilatometer (see Part I) is constructed using pieces of the host and inclusion minerals being studied. This device is designed to monitor a *set* of isomekes passing through a *P-T* region that is sufficiently large to include any possible values of P_f and T_f. Each isomeke, by definition, shares the property that it is a *P-T* trajectory for which the length of an appropriately oriented line segment between two points of reference[6] embedded in a piece of the inclusion mineral equals that between similarly defined points in a piece of the host mineral. Secondly, let some laboratory pressure (P_n) and temperature (T_n) be found for which the piezobirefringent halo around the inclusion in the host is observed to vanish. The isomeke passing through P_f, T_f is then that particular isomeke passing through P_n, T_n. The intersection of that isomeke with another, independently determined for some other host-inclusion combination in the specimen, uniquely specifies P_f, T_f, assuming that both combinations formed under the same conditions.

Relationship of Solid Inclusion Piezothermometry to Equations of State

Because equations of state provide an alternate means for the determination of isomekes, it is desirable to clarify their interrelationship.

Let the *natural strain* (Nadai, 1950, p. 73–74) $\bar{\epsilon}$ between two points of reference embedded in a given solid be defined as

$$\bar{\epsilon} \equiv \ln\left(\frac{l}{l_0}\right) = \ln(1 + \epsilon) \qquad (1)$$

where

$l \equiv$ distance between the points at some *P* and *T*

$o \equiv$ subscript indicating standard conditions, $P = 1$ bar and $T = 25°C$, *not* necessarily on a desired isomeke.

---

[4] Rosenfeld (1969, p. 320–326, 330) makes applications based on the two-dimensional approach, which entails relaxation by thin-sectioning of some or all of the elastic strain due to deviatoric stress. Determination of the angular relations for elimination of that strain is an essential feature of the method. That this approach can only be approximate when dealing with noncubic minerals results from the necessarily finite thickness of the thin section, the irregular shapes of real inclusions, and the possible presence of shear stresses parallel to the host-inclusion contact.

[5] As an example, let θ be the angle between the section normal and *c* of a uniaxial inclusion (*e.g.,* quartz) in an optically isotropic host (*e.g.,* garnet). A *P-T* region will exist for which the condition of appearance of a piezobirefringent halo at a particular *P* and *T* is $\theta > \theta_c$, where θ_c is the limiting value of θ for which a halo appears (Rosenfeld, 1969, p. 320–323).

[6] The line segments connecting the reference points in each piece also must parallel the crystallographic directions within host and inclusion for which the strains are equal in the conceptual model. While it is simple to identify these directions for minerals of high symmetry (see, for example, Rosenfeld, 1969, p. 318–327), a general procedure that is also applicable to minerals of the least symmetric crystal systems has not yet been developed.

$$\epsilon \equiv \frac{l - l_0}{l_0} \equiv \text{the } conventional \text{ } strain.$$

Then the natural strain difference, δ_{x-y}, between the line segments connecting two reference points embedded in solid x and two reference points embedded in solid y at some arbitrary P and T is

$$\delta_{x-y} \equiv \bar{\epsilon}_x - \bar{\epsilon}_y \qquad (2)$$

Now an isomeke, by definition, is a curve in P and T along which two reference points embedded in x remain the same distance apart, l_x, as that between two reference points embedded in y, l_y, or

$$l_x = l_y \qquad (3)$$

The location of the isomeke is uniquely determined by the ratio of l_y to l_x at standard conditions, l_{y0}/l_{x0}, which is a constant, not necessarily equal to unity, for a given isomeke. To see this, from Equation (1) we obtain

$$\ln l_x = \bar{\epsilon}_x - \ln l_{x0} \qquad (4a)$$

$$\ln l_y = \bar{\epsilon}_y - \ln l_{y0} \qquad (4b)$$

Subtracting Equation (4b) from (4a) and using Equations (2) and (3), we find

$$\delta_{x-y} = \ln \left(\frac{l_{y0}}{l_{x0}} \right). \qquad (5)$$

δ_{x-y} is thus constant along a given isomeke and can, in principle, be determined at standard conditions by measuring l_{x0} and l_{y0}. From Equation (2) the relationship between an isomeke and the equations of state of two solids is also evident. An isomeke is found to be any curve in P and T along which the difference in natural strain is constant. Thus a good graphical way to see the functional relationship between isomekes and equations of state is a P-T diagram with contours of constant natural strain. The superposition of such diagrams for x and y allows determination of isomekes by a simple procedure. Each isomeke is a contour of constant difference, δ_{x-y}, in natural strain.[7] If, eventually, an accurate way for measuring δ_{x-y} can be incorporated into our system of comparison dilatometry and the equation of state of x is known, it follows from Equation (2) that $\bar{\epsilon}_y$ can be determined all along the isomeke characterized by that δ_{x-y} by subtraction of δ_{x-y} from $\bar{\epsilon}_x$. The equation of state of y could thereby

---

[7] The method of plotting isomekes is identical to that used by geologists in plotting convergence maps, maps showing contours of constant vertical component of thickness of a stratigraphic unit (Lahee, 1941, p. 649–654).

be determined by generation of suitably spaced isomekes.

The differential equation of an isomeke also follows from Equation (2). The total differential of δ_{x-y} is

$$d\, \delta_{x-y} = \left(\frac{\partial\, \delta_{x-y}}{\partial T} \right)_P dT + \left(\frac{\partial\, \delta_{x-y}}{\partial P} \right)_T dP \qquad (6)$$

At constant δ_{x-y},

$$m_{x-y} \equiv \left(\frac{\partial T}{\partial P} \right)_{\delta_{x-y}} = -\frac{(\partial\, \delta_{x-y}/\partial P)_T}{(\partial\, \delta_{x-y}/\partial T)_P}$$

$$= \frac{-[(\partial \bar{\epsilon}_x/\partial P)_T - (\partial \bar{\epsilon}_y/\partial P)_T]}{(\partial \bar{\epsilon}_x/\partial T)_P - (\partial \bar{\epsilon}_y/\partial T)_P} = \frac{\beta_x - \beta_y}{\alpha_x - \alpha_y} \qquad (7)$$

where β and α are, respectively, the isothermal linear compressibility and isobaric linear coefficient of thermal expansion, both simply defined as partial derivatives of $\bar{\epsilon}$.

There is ample reason, therefore, to use $\bar{\epsilon}$-P-T diagrams in analyzing data from comparison dilatometry.

Calibration for Association Quartz-Garnet

The previous calculation of families of isomekes (Rosenfeld, 1969, p. 327–334; there called "integral null curves" or "isogons") for almandine–quartz was based on the very scant data on α's and β's and on long-range extrapolation using more-or-less reasonable boundary conditions.

We present here the experimental calibration of the association quartz (q)–garnet (g), emphasizing garnet of the almandine type (garnet #1, in Table 1 and Fig. 1). Limited experiments on other garnets, whose compositions are also shown in Table 1 and Figure 1, allow some generalization about the effect of solid solution on the almandine-quartz isomekes. All garnets were analyzed by electron microprobe.

Experimental Results

Results for Pair: Quartz–Almandine-Type Garnet

Figures 2, 3, and 4 show data points within the region bounded by the low-high quartz transition and 7 kbar for isomekes of almandine-type garnet (garnet #1) relative to quartz. In Figure 2 the quartz rod is oriented $\perp c$; in Figure 3 it is oriented at an angle of 45° relative to c; and in Figure 4 it is oriented $\parallel c$. The curves in these figures are derived as described in a section below. For convenience in petrographic utilization (Rosenfeld, 1969, p. 327–328), the curves are identified by $\sin^2\theta$, where θ is the angle between

TABLE 1. Compositions of Garnets Studied

	1	2	3	4	5	6
Weight percent oxides						
SiO_2	37.77	38.25	43.04	42.30	36.43	39.23
TiO_2	0.00	0.00	0.38	0.14	0.00	0.19
Al_2O_3	21.11	21.55	22.94	22.19	20.64	21.80
Cr_2O_3	0.00	0.04	0.18	1.89	0.00	0.00
FeO	35.11	26.09	10.17	8.84	18.65	1.84
MnO	2.24	2.32	0.30	0.35	24.29	0.45
MgO	4.53	9.47	19.02	19.03	0.00	0.00
CaO	0.39	1.92	4.87	5.16	0.32	34.76
Total	101.15	99.64	100.90	99.90	100.33	98.27
Number of ions on the basis of 12 oxygens						
Si	3.00	2.97	3.04	3.02	3.00	3.01
Al	1.97	1.97	1.91	1.87	2.00	1.97
Cr	0.00	0.00	0.01	0.11	0.00	0.00
Ti	0.00	0.00	0.02	0.01	0.00	0.01
Mg	0.54	1.10	2.00	2.03	0.00	0.00
Fe^{2+}	2.33	1.69	0.60	0.53	1.28	0.12
Mn	0.15	0.15	0.02	0.02	1.69	0.03
Ca	0.03	0.16	0.37	0.40	0.03	2.86
	3.05	3.10	2.99	2.98	3.00	3.01
Mol. percent components						
$Fe_3Al_2Si_3O_{12}$	76.39	54.52	20.23	19.16	42.67	3.99
$Ca_3Al_2Si_3O_{12}$	0.98	5.16	11.40	2.71	1.00	95.02
$Mg_3Al_2Si_3O_{12}$	17.70	35.48	67.43	73.49	0.00	0.00
$Mn_3Al_2Si_3O_{12}$	4.92	4.84	0.60	0.77	56.33	1.00
$Ca_3Cr_2Si_3O_{12}$	0.00	0.00	0.34	3.87	0.00	0.00

1. Almandine -- Source : F. Birch; locality unknown
2. Pyropic Almandine -- U.S.N.M. #120315, Fort Defiance, Arizona
3. Pyrope -- U.S.N.M. #107062, Alice Springs, Australia
4. Cr-Pyrope -- UCLA Museum 3227D, Arizona
5. Spessartitic Almandine -- Verma #1 (Verma, 1960)
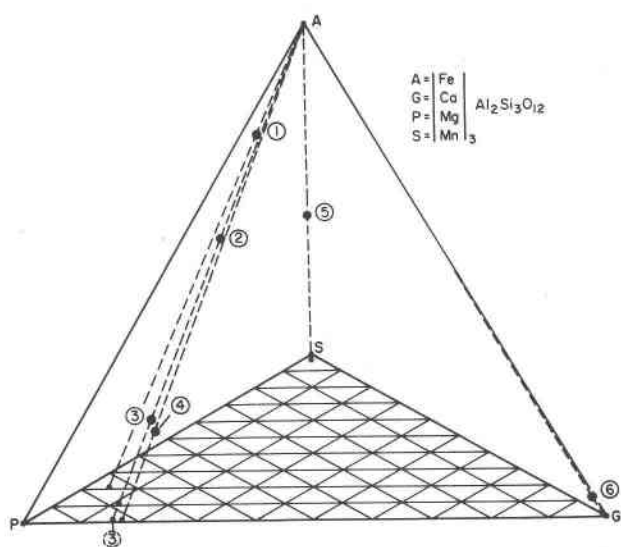6. Grossular -- Asbestos, Quebec (J. Arem, Collector).

FIG. 1. Compositional tetrahedron for garnets used in comparison dilatometry. Numbers correspond to chemical analyses listed in Table 1.

the axis of the rod and the $\perp$ to c (*i.e.*, for quartz $\perp c$ $\sin^2\theta = 0$). It is easily seen that, in applying these results to thin sections, θ is the same angle as θ in the comparison dilatometry (see footnote 5).

Results for Pairs: Quartz and Pyropic, Spessartitic, and Grossularitic Garnet

Figures 5, 6, and 7 show data points for isomekes of quartz in the two principal orientations relative to pyropic (Table 1, #3), spessartitic (#5), and grossularitic (#6) garnets. Similar determinations, not illustrated because they are concordant, were made for garnets #2 and #4 of Figure 1 and Table 1. The solid curves in Figures 5, 6, and 7 are derived from interpolation equations presented below for isomekes of quartz–almandine-type garnet and are placed in the figures for purposes of comparison.

Discussion and Synthesis

The most useful results to petrology that stem from this comparison dilatometry are: (1) experimentally-
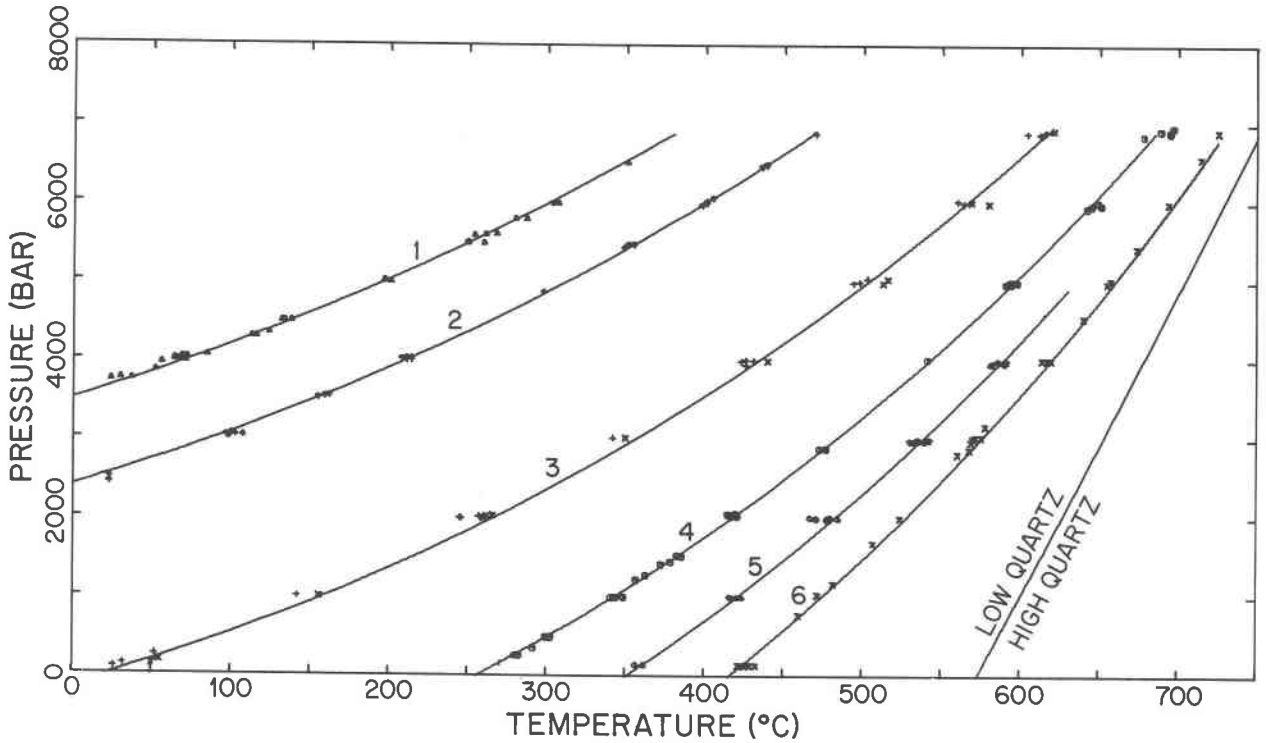
FIG. 2. Data for isomekes between almandine-type garnet (No. 1 in Table 1) and quartz in a direction ⊥c. Solid lines based on numerical analysis discussed in text. Type of dilatometer (see Part I) used: 1, 2, 4, 5-"gate" (antimony-doped silicon gate); 3-"gate" (gate of chrome-coated synthetic sapphire); 6-"gate" (WC gate).
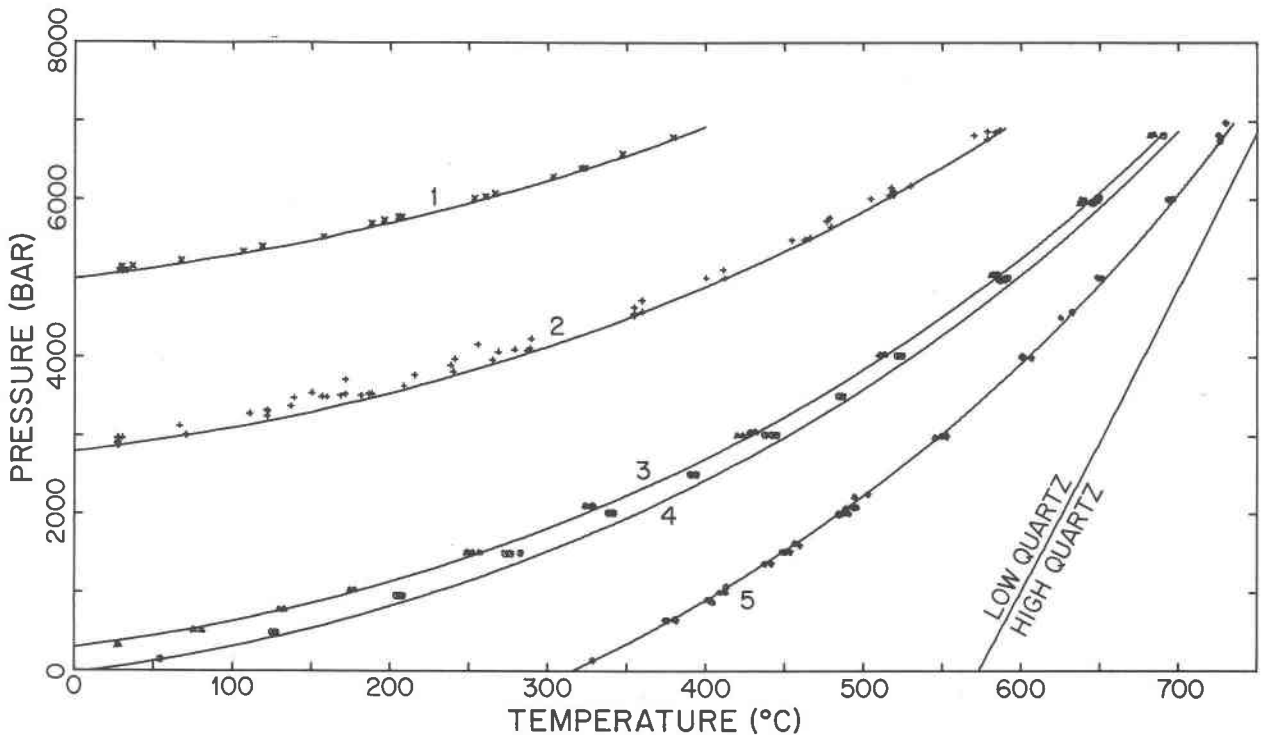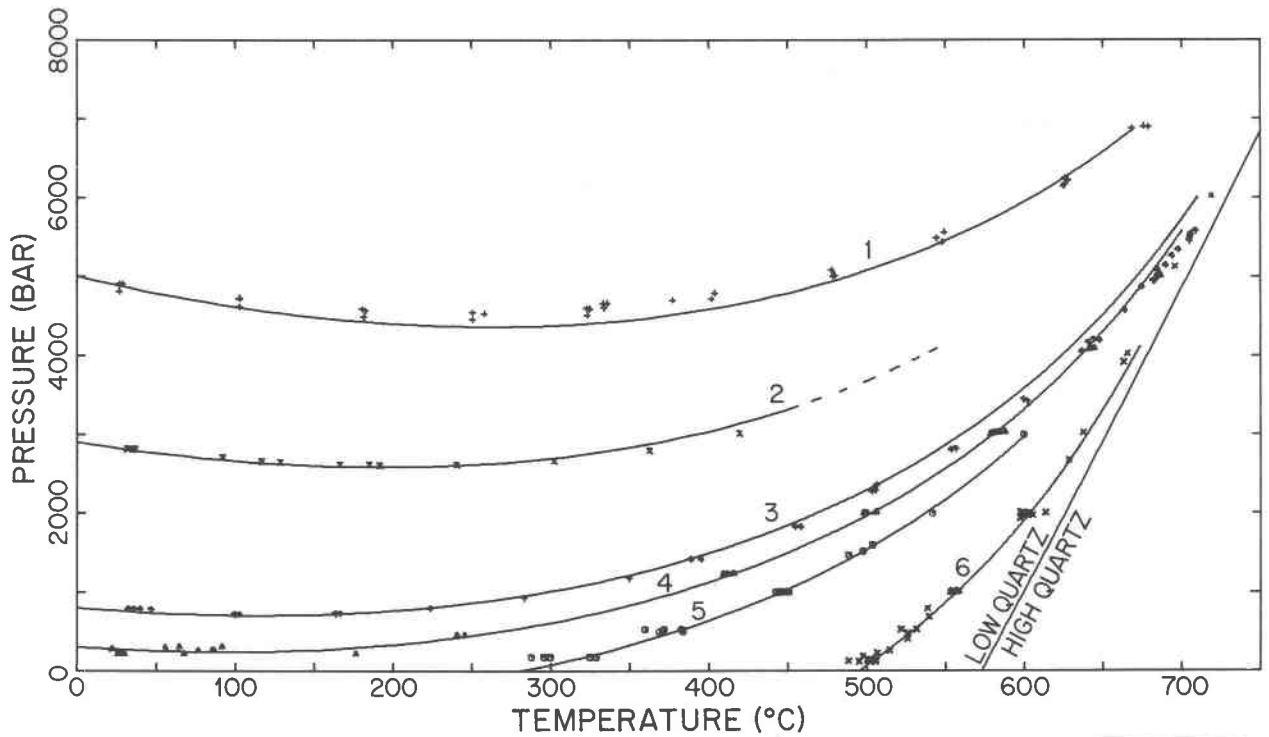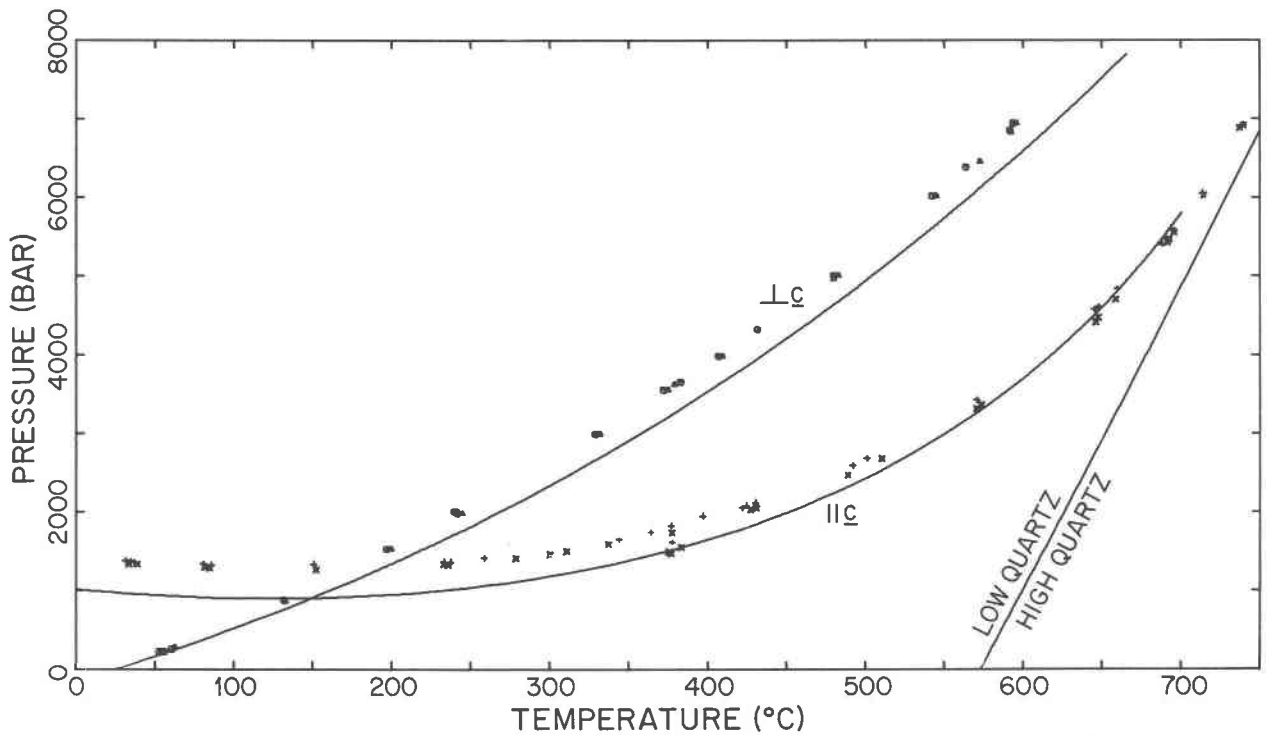

FIG. 3. Data for isomekes between almandine-type garnet (No. 1 in Table 1) and quartz in a direction 45° from c. Solid lines based on numerical analysis discussed in text. Type of dilatometer used: 1, 2, 5-"gate" (WC gate); 3, 4-"J".

FIG. 4. Data for isomekes between almandine-type garnet (No. 1 in Table 1) and quartz $||c$. Solid lines based on numerical analysis discussed in text. Type of dilatometer used: 1, 5-"gate" (antimony-doped silicon gate); 2, 3, 4-"J"; 6-"gate" (WC gate).

FIG. 5. Data for isomekes between pyropic garnet (No. 3 in Table 1) and quartz $\perp c$ and $||c$ using "gate" dilatometer (WC gate). Solid lines for comparison are derived from interpolative equations for quartz and almandine-type garnet.
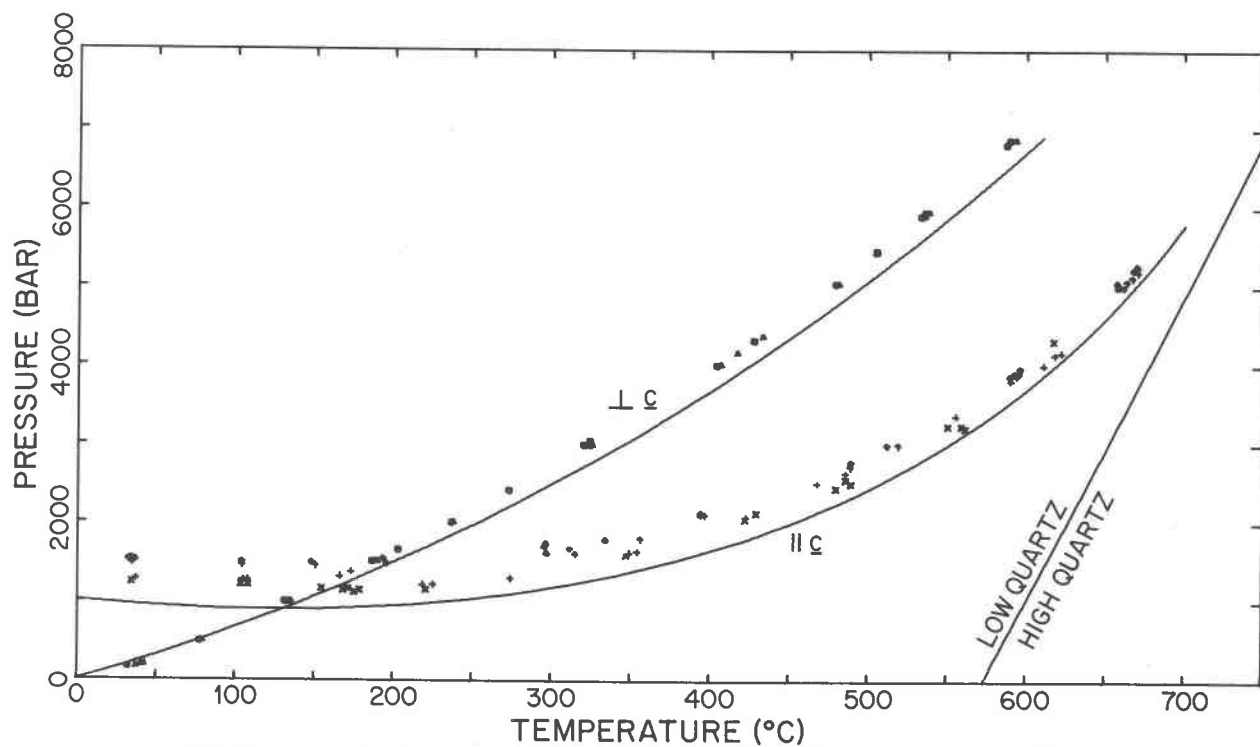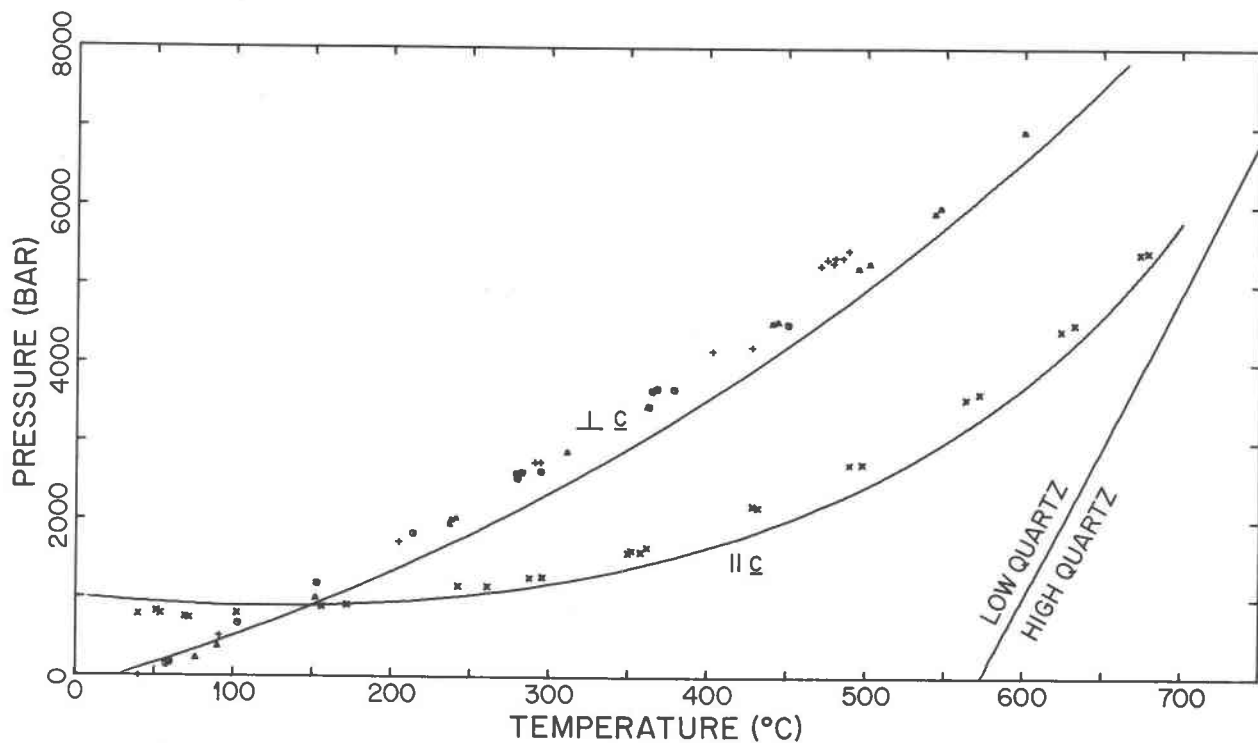
FIG. 6. Data for isomekes between spessartitic almandine (No. 5 in Table 1) and quartz ⊥c and ||c using "gate" dilatometer (WC gate). Solid lines for comparison are derived from interpolative equations for quartz and almandine-type garnet.

FIG. 7. Data for isomekes between grossular (No. 6 in Table 1) and quartz ⊥c and ||c using "opposed rods" dilatometer. Solid lines for comparison are derived from interpolative equations for quartz and almandine-type garnet.

determined isomekes for the almandine-quartz combination; and (2) the demonstration that extreme variations in composition of garnet cause only small variations in the trajectories of the isomekes. Referring to Equation (7), the minor effect of major compostional departures probably reflects the fact that the changes, respectively, in α_g and β_g due to compositional variation at any P and T are small relative to $(\alpha_q$-$\alpha_g)$ and $(\beta_q$-$\beta_g)$ at the same P and T. This contrast in the properties of garnet and quartz, besides increasing sensitivity, thus becomes another asset of this pair of minerals for solid inclusion piezothermometry. The petrologist using the pair garnet-quartz will, for most occurrences, be working with garnets much closer to almandine than to the other garnets considered. It should therefore be justifiable for him to use isomekes derived for quartz and almandine-type garnet with only approximate determination that he is dealing with this type of garnet.

One additional conclusion from this work is the large difference between coefficients of thermal expansion of garnet, deduced below, and those obtained by X-ray diffraction on synthetic garnets (Skinner, 1956). Near 25°C and 1 bar, the data for one isomeke in Figure 4 very nearly parallel the temperature axis. Using the known properties of quartz referred to in Part I and the compressibility of almandine-type garnet (designated by a), $\beta_a = 0.189 \times 10^{-6}\text{bar}^{-1}$ (Soga, 1967), Equation (7) suggests that, near 25°C and 1 bar,

$$\alpha_{q\|c} \approx \alpha_a \approx 7.56 \times 10^{-6} \text{ °C}^{-1}.$$

Using this same equation, the compressibility of spinel (s), β_s mentioned in Part I, our calculated value of $\alpha_{s0} = 5.72 \times 10^{-6}$ °C^{-1}, and the slope of an isomeke for the same garnet relative to spinel at its intercept with the temperature axis (60°C instead of 25°C), we obtain $\alpha_{a0} = (7.58 \pm 0.14) \times 10^{-6}$ °C^{-1}. There is close agreement between our two independently determined values, which are ~39 percent larger than thermal expansions derived from the X-ray work of Skinner (1956) on synthetic almandine.

The differences between the previous data on thermal expansion for garnet and values inferred above account for the marked discordance between the calculated isomekes of Rosenfeld (1969) and those presented in this paper. Revised geological interpretations based upon the correct measurements are discussed below.

Representation and Interpolation of Experimental Results

Were satisfactory equations of state for almandine and low quartz available, smoothing of experimental data and presentation of results would be easily accomplished utilizing these equations in the manner previously discussed. No such equations of state, valid throughout the pressure and temperature region of our experimentation, have been advanced. Much of the theoretical problem lies with changes in physical properties which are precursors to the low-high transition of quartz; some of these precursory phenomena are readily detected more than 75°C below the transition (Klement and Cohen, 1968).

Empirical methods were thus used to smooth and present the quartz-almandine data. The technique presented here yielded a relatively simple representation which, although suitable for geological applications, is not suitable for accurate equations of state.

The empirical equation is an excellent fit to the data for quartz $\perp$ c–almandine and quartz 45° to c–almandine; the empirical equation fits the quartz $\|c$–almandine data with less precision, although suitably for petrological purposes, to within 75° of the low-high transition. Progressive deviation of the empirical equation from the experimental data within ~75°C of the transition undoubtedly is an artifact of the mathematical form and simplicity of the equations.

The desired equation should generate isomekes as a function of temperature, pressure, and orientation of quartz. No single integrated equation was found to do this, although a differential equation was. The calculated quartz-almandine isomekes were thus obtained by numerical integration of

$$\frac{dP}{dT} = a_1 + a_2 P + (a_3 + a_4 P) \ln (T_\lambda - T) \qquad (8)$$

where

$$a_1 = 56.391 + 13.323 \quad \sin^2\theta \quad - 23.646 \quad \sin^4\theta \qquad (9a)$$

$$a_2 = -9.241 \times 10^{-4} \quad -4.881 \times 10^{-3} \quad \sin^2\theta \\ +7.718 \times 10^{-3} \quad \sin^4\theta \qquad (9b)$$

$$a_3 = -7.948 - 3.011 \quad \sin^2\theta \quad + 3.526 \quad \sin^4\theta \qquad (9c)$$

$$a_4 = 2.147 \times 10^{-4} + 7.634 \times 10^{-4} \quad \sin^2\theta \\ -1.333 \times 10^{-3} \quad \sin^4\theta \qquad (9d)$$

and

$$T_\lambda = 573.2 + 0.02683P - 0.1435 \times 10^{-6}P^2 \quad (10)[8]$$

P is in bars and T in °C.

Briefly, coefficients in Equation (8) were obtained by numerical techniques as follows: The experimental data for one isomeke were ordered in ascending temperature or pressure, depending upon the slope of the isomeke. An arbitrary interval of 25°C was chosen, and data points which are separated by a distance greater than or equal to this arbitrary interval were selected by the computer starting from the lowest temperature or pressure. This ordered set was the basis of all succeeding calculations.

Next, the derivative of the isomeke, dP/dT_i, was found at each point T_i in succession by the Lagrangian interpolation polynomial of degree 2. Except at the end points, dP/dT_i was obtained using T_i and the adjacent higher and lower temperature points. The derivatives at the end points were found from the first three and last three points.

Each experimental determination of an isomeke was processed in this manner. All dP/dT values for isomekes involving a specific orientation of quartz were then grouped together and a smooth surface of the form of Equation (8) best fit by least squares analysis. For each of the three orientations of quartz utilized in the experiments, values of a_1, a_2, a_3, and a_4 were found. Thus 12 coefficients were determined. Finally, a quadratic equation was fitted to each coefficient a as a function of the orientation of the quartz, θ. These quadratics are given in Equations (9a-9d).

The isomekes for almandine together with any arbitrary orientation of quartz were then obtained by standard numerical integration techniques using Equation (8). These curves, spaced at intervals of 0.2 in $\sin^2\theta$, are given in Figure 8. Also, Figure 9 is a "fan" of isomekes emanating from $P = 1$ bar and $T = 25$°C at intervals of 0.1 in $\sin^2\theta$ for petrographic convenience (see footnote 5; also *cf* Rosenfeld, 1969, p. 334–345).

A number of equations other than Equation (8) were examined to obtain a representation of all the data. Some utilized functions other than $\ln (T_\lambda - T)$; others utilized additional terms. No consistently better representation was found to fit *all* the data, although some may have yielded better representations in limited regions. Some equations with more coefficients may have fit the data just as well, but the simpler equation was chosen for presentation here. The $\ln(T_\lambda - T)$ term allows presentation of an equation of simple form that approximates our data. This logarithmic term, however, has no particular theoretical basis and its behavior may cause deviations from a good fit to the quartz $\|c$-almandine data. Caution should be used in applying Equation 8 outside the region within which which we have applied it.

Geological Applications

Ideally one should be able to use solid inclusion piezothermometry alone to determine $P - T$ conditions of metamorphism; the most precise such determinations would employ location of isomekes crossing at relatively high angles. For example, using thin sections of garnets with quartz inclusions in conjunction with Figure 8, such high-angle intersections would require finding conditions for elimination of birefringent halos around quartz grains having both low and high inclinations, θ, of the c axis to the section normal. When applying solid inclusion piezothermometry to location of the Al_2SiO_5 triple point, commercially available heating stages are suitable for determining such null conditions for quartz grains with low θ. To obtain null conditions with quartz grains having high θ, however, requires use of a high aperture window bomb. Thus, pending completion of such an optical high pressure device, we have not been able to investigate null conditions of halos for grains with values of θ sufficiently far apart to give accurate "triangulation" in $P - T$ space.

Instead of using piezobirefringent halos around quartz inclusions in garnet alone, we have thus been forced to combine their use with additional petrological data as was done by Rosenfeld (1969, p. 335–345) to infer pressures and temperatures of crystallization. In that paper isomekes were generated using the limited information on coefficients of compressibility and thermal expansion then available. For any particular temperature, the pressures implied in Figure 8 of that paper are higher than they would be using the isomekes of Figure 9 in this paper. The discrepancies, though not large (~1.5 kbar), result largely from coefficients of thermal expansion previously available for garnet, coefficients

---

[8] From preliminary work on the low-high quartz transition. More extensive work (Cohen, Klement, and Adams, 1974) suggests that the coefficient of the P^2 term may be negligible and that slight alteration in the coefficient of the P term may be appropriate. Such modifications have no significant effect on our results.
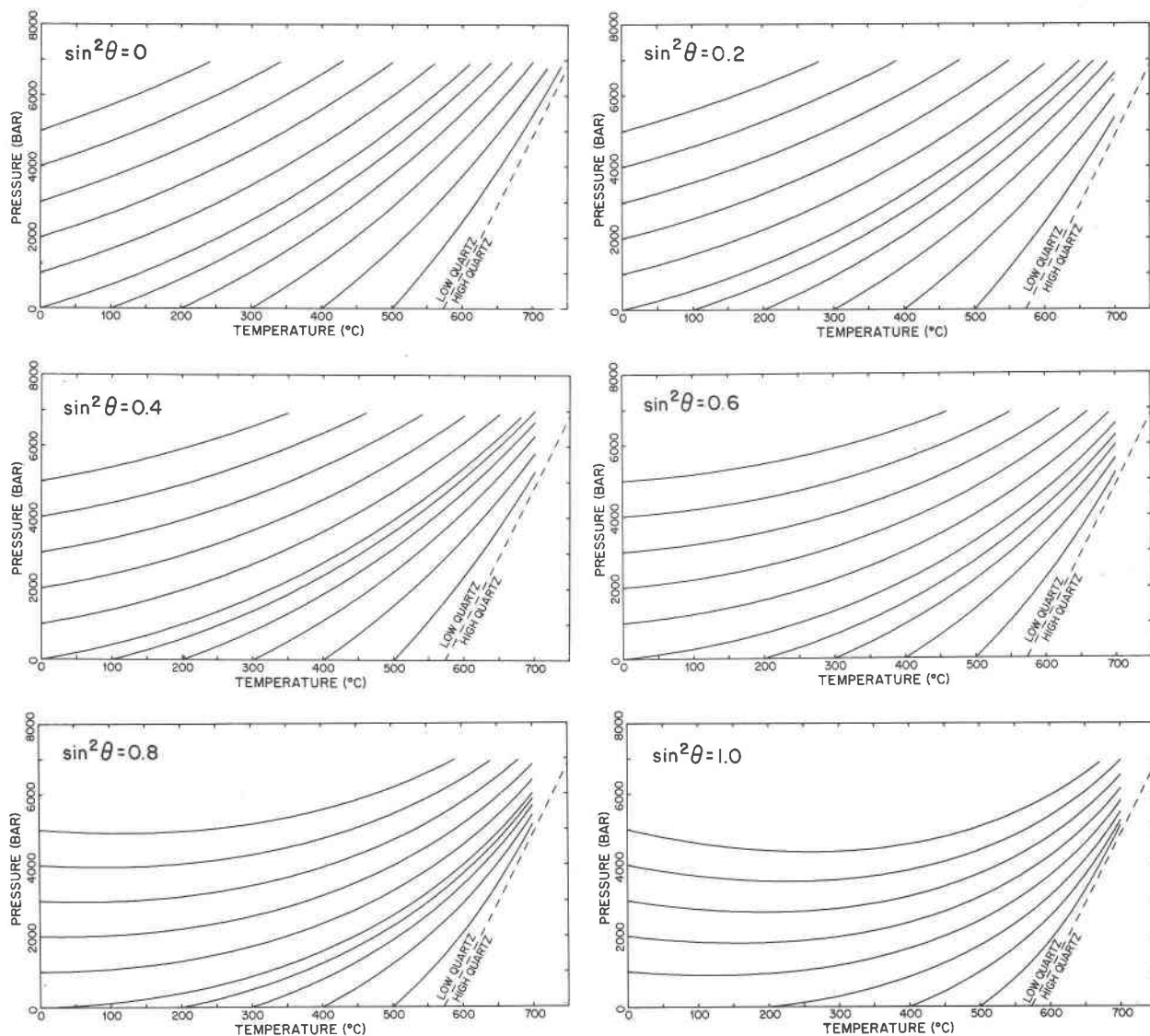
FIG. 8. Calculated sets of isomekes at intervals of 0.2 in $\sin^2\theta$: almandine-type garnet and quartz.

that we now believe are too low as a result of experiments reported above. Figure 10 updates the most critical parts of his illustration for localities in New England and includes new information from the southern Gotthard Region in Switzerland.

Figure 10 applies the data presented here to garnet-quartz combinations from areas selected to yield information bearing on Al_2SiO_5 polymorphism. Restrictions on the location of the andalusite-kyanite-sillimanite triple point are inferred as follows:

(1) Specimen Gar. 1 is a kyanite-bearing para-gonite schist from the well-known locality of Gassetts, Vermont, that (a) is located in the kyanite zone many miles from any known contemporaneous sillimanite (Thompson and Norton, 1968, p. 320); (b) shows, using the two-dimensional approach, weak piezobirefringent halos in almandine around quartz inclusions having $\theta = 0°$; (c) is isogradic with marble, cropping out 4.13 km to the north in Duttonsville Gulf (Thompson and Norton, 1968, p. 320), that consists mostly of dolomite with minor calcite having 5.8 mole percent $MgCO_3$ [9](Rosenfeld, 1969, p. 343); (d)

---

[9] This composition includes thin dolomite lenses that show evidence of exsolution because they are oriented normal to c of the host calcite, they extinguish under crossed polars parallel to the host calcite, and they have a graded range of coarseness that is of finer grain than that of the dolomite of the matrix.
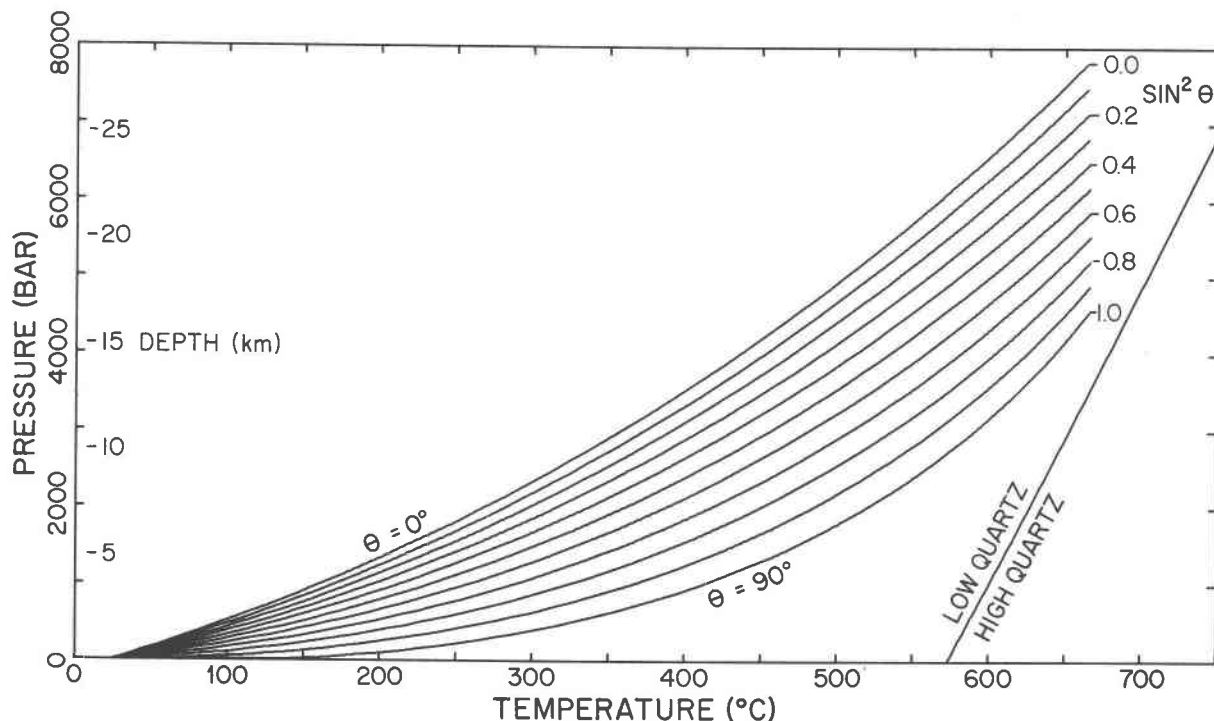
FIG. 9. Calculated "fan" of isomekes between almandine-type garnet and quartz, emanating from $P = 1$ bar and $T = 25°C$ at intervals of 0.1 in $\sin^2\theta$.

has, in an adjacent sample, the following $\Delta O^{18}/O^{16}$ values (Garlick and Epstein, 1967, p. 192–193, 212) between quartz and the minerals indicated: 3.0 (muscovite), 4.3 (garnet), 5.0‰ (biotite). Utilization of (a), (b), (c), Figure 9, and interpolated isopleths for $MgCO_3$ solubility in calcite obtained from the experimental data of Goldsmith and Newton (1968) places kyanite in a small $P - T$ region above 5.6 kbar at a temperature of $545 \pm 20°C$. This temperature, in turn, calibrates facts (d)[10], to be used below.

(2) Specimen A57d is from the Silurian Clough quartzite in the eastern highlands of Connecticut (Garlick and Epstein, 1967, p. 214). Specimen A57d (e) is very near the kyanite-sillimanite isograd 0.44 km northeast of an outcrop of kyanite schist and 0.43 km north-northwest of one of sillimanite-bearing schist; (f) indicates recrystallization temperature very nearly the same, within the precision of measurement, as that of specimen Gar. 1, because the following $\Delta O^{18}/O^{16}$ values (Garlick and Epstein, 1967, p. 214) between quartz and the minerals indicated are close to those of specimen Gar. 1: 3.0 (muscovite), 4.4

---

[10] The work of Clayton, O'Neill, and Mayeda (1972, p. 3064) leaves the earlier experimental calibrations of the O^{18}/O^{16} geothermometer based on fractionation between quartz and muscovite in a very uncertain state.
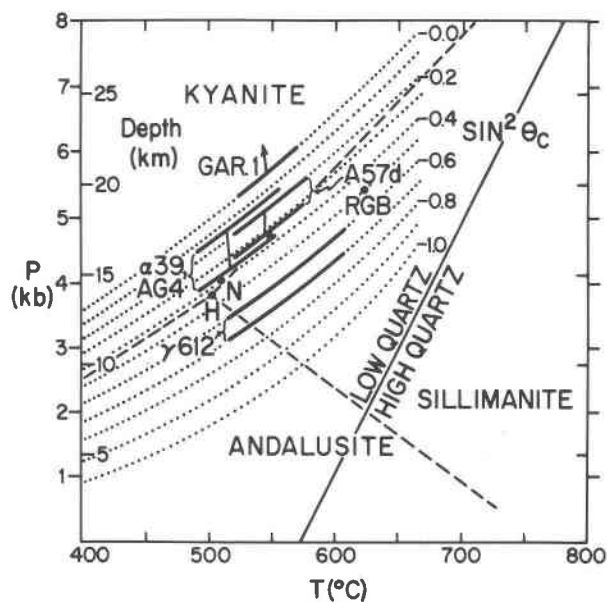

FIG. 10. Geological application of solid inclusion piezothermometry using the garnet-quartz combination. See text for specimen locations and discussion. Dotted isomekes are from Figure 9. Heavy lines indicate range of uncertainty for each specimen. Steep lines attached to heavy lines represent geochemically determined information on temperature of crystallization. Dashed lines are subdivisions of the Al_2SiO_5 diagram after Holdaway (1971). Triple point determinations within that diagram: H = Holdaway (1971); N = Newton (1966); RGB = Richardson et al (1969).

(garnet), 5.9‰ (biotite); (g) has values of $\sin^2\theta_c$, at atmospheric pressure, of 0.2 to 0.32 at 25°C and 0.06 at 90 ± 15°C (new values from Adams, 1971, p. 87–90). Utilization of (e), (f), (g), and Figure 9 indicates that kyanite crystallized near the sillimanite field in a small $P - T$ region near 5 kbar and 545 ± 20°C, in quite good accord with placement of the kyanite-sillimanite boundary by both Newton (1966) and Holdaway (1971, p. 115). Thus we infer that the triple point should lie at a temperature below 545°C along a curve governed by the Clapeyron equation that emanates from $T \sim 545°C$ and $P \sim 5$ kbar.

(3) Specimens $\alpha39$ and AG4 are from the vicinity of the south border of the Gotthard Massif near Lukmanier Pass, Tessin, Switzerland. $\alpha39$ is from the Triassic Quartenschiefer near the small hamlet of Brönich; and AG4 is from pre-Triassic schist of the Lukmanier-Decke immediately south of Passo del Sole, about 5 km west of Brönich. Specimen $\alpha39$, a quartz-bearing paragonite schist, (h) shows, by abundant porphyroblasts of kyanite and oligoclase ($\sim An_{18}$), that the reaction leading to production of kyanite was: paragonite + quartz → kyanite + plagioclase + H_2O; (i) indicates, by the relationship of trains of inclusions inside porphyroblasts to their continuation outside, that the porphyroblasts formed late in the last major deformation that accompanied the metamorphism; (j) has some kyanite porphyroblasts that are bent up to 60° and have reac-
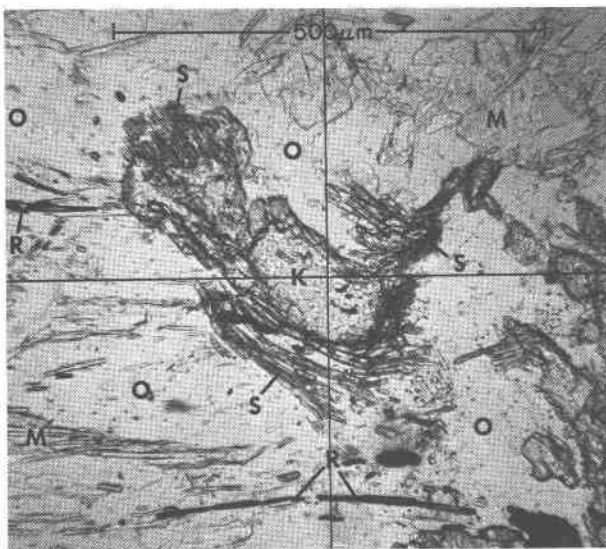

FIG. 11. Bent kyanite porphyroblast surrounded by selvage of sillimanite needles in paragonite schist from vicinity of Brönich in the Lukmanier Pass region, Switzerland. Minerals: K = kyanite; S = sillimanite; O = oligoclase; M = white mica; R = rutile.

tion selvages of sillimanite needles that are also bent, but to a lesser degree, about the same axis (Fig. 11); (k) was located near a paragonite-muscovite schist in which $d_{002\ muscovite}$ = 9.929 Å (Frey, 1969, p. 126). We infer from (i) and (j) that the incomplete reaction kyanite → sillimanite occurred after dehydration reaction (h) that produced the kyanite porphyroblasts and therefore *after* the thermal maximum. If the reaction kyanite → sillimanite had taken place *before* the thermal maximum, dispersed and relatively coarse sillimanite should have been formed by the dehydration reaction instead of kyanite. Inasmuch as this is not the case, we infer that sillimanite formed primarily as a result of unloading and not as a result of rising temperature. Based on Rosenfeld *et al* (1958), we infer that the solid solution between muscovite and paragonite, reflected in basal spacings, indicates the *maximum* temperature of metamorphism. For that association, Rosenfeld (1969, p. 343–344) calibrated $d_{002,\ muscovite}$ against $MgCO_3$ concentrations in calcite of closely juxtaposed dolomitic marbles. This enables use of fact (k) above to select the correct isopleth for $MgCO_3$ solubility in calcite from the experimental work of Goldsmith and Newton (1968), in this case 4.9 percent. Intersection of this isopleth with an isomeke obtained from isogradic specimen AG4 (see metamorphic map of Niggli, 1970, p. 18–19), yields the temperature and pressure of crystallization. Observation shows that isomeke to have a value of $\sin^2\theta_c$ between 0.14 and 0.35 using Figure 9. The intersection (Fig. 10) lies in a small $P - T$ region near 4.3 kbar near 515 ± 25°C.

(4) The discussion of specimen $\gamma612$ from Gap Mountain, New Hampshire, is unchanged from Rosenfeld (1969, p. 340–343) except for recalibration of isomekes. In $\gamma612$, which has $\sin^2\theta_c$ between 0.6 and 0.7, there is evidence of the reaction andalusite → sillimanite. This is consistent with the results of Holdaway in that those isomekes intersect his andalusite-sillimanite boundary. The data for $\gamma612$ are not so restrictive as the combined results for specimen A57d and the alpine specimens.

In summary, the information from the Alps not only is consistent with location of a pressure and temperature on the kyanite-sillimanite boundary in New England but is probably more restrictive on the temperature of the triple point. What makes the Alpine information of most interest is the above inference that the reaction kyanite → sillimanite took place at or below approximately 515°C. The sillimanite in the southern Gotthard area is 25 km from

the nearest point on the sillimanite isograd to the southeast (Niggli, 1970, plate 2). Its occurrence is probably a result of a curious set of circumstances: activation of recrystallization by strain energy of deformation coupled with relatively rapid unloading due to denudation that accompanied the formation of the central Alps as a range of high mountains after the Eocene (Niggli, 1970, p. 18). The rapidity of unloading relative to cooling by thermal conduction apparently maintained temperatures sufficiently high for the reaction to take place when the $P - T$ path of the rock entered the sillimanite field on its way to the lower P and T at the earth's surface.[11] Assuming that there are no problems with metastable crystallization of sillimanite relative to andalusite in the geological time intervals involved, the triple point must lie at $T < (515 \pm 25°C)$. Examination of Figure 10 shows that the experimentally inferred triple points of Newton (1966) and of Holdaway (1971, p. 115) lie within the $P - T$ region below 515°C between temperatures on the isomekes for specimens A57d and AG4 or α39 on the high-P side and specimen γ612 on the low-P side. This is consistent with the above inferences from solid inclusion piezothermometry and geochemistry. The triple point of Richardson, Gilbert, and Bell (1969, p. 266) lies at too high a temperature to be consistent with the above interpretations.

The information from specimens α39 and AG4 in Figure 10 also provides information on the average denudation rate since the thermal maximum in the area. Clark and Jäger (1969, p. 1149) place the thermal maximum in the area at (30 ± 5) m.y., consistent with the work of Steiger (1964). Denudation of $\sim$16 km of material (inferred from the 4.3 kbar pressure of crystallization) during that interval leads to a mean denudation rate of 0.5 ± 0.1 mm/year. This rate is closely comparable with inferred denudation rates of Clark and Jäger (1969, p. 1154) for the area of the Gotthard Tunnel a few kilometers to the west of Passo del Sole along the structural trend. They interpreted a relatively high heat flow there as a transient effect of denudation.

Epilogue

Full application of solid inclusion piezothermometry awaits completion of a high aperture window bomb to complement a heating stage in finding conditions for halo elimination. Using the heating stage and window bomb, it should become possible to cross-check answers obtained totally by solid inclusion piezothermometry against those obtained by other means.

The possibility of plastic deformation around or in an inclusion must be considered. Carstens (1971) has demonstrated creep around inclusions in mantle-derived garnet xenocrysts that must have followed a $P - T$ path which, at high temperature, greatly and rapidly departed from the relevant isomekes (*cf* Rosenfeld and Chase, 1961, p. 538). It remains to be seen whether such plastic deformation is important in regionally metamorphosed crustal rocks that recrystallized at much lower temperatures and that probably followed $P - T$ paths having much lower departures from relevant isomekes over much longer time intervals. It is even possible that quantitative experimental and theoretical analysis of dislocation halos, such as those noted by Carstens, might yield information on original conditions of formation and/or unroofing history.

The work we report here is thus somewhat in the nature of a progress report. Further experimental determinations of isomekes are needed—*e.g.,* sillimanite-garnet, diamond and its inclusions—and some are in progress. Further instrumentation will have to be developed—*e.g.,* the window bomb—and this is also in progress; and further work will be necessary on dislocation creep and the theoretical foundations of solid inclusion piezothermometry.

Acknowledgments

---

[11] That this phenomenon is not unique in the region is indicated by the textural evidence in a specimen collected 12 km to the south. There, in a specimen of the higher temperature paragonite-muscovite ($d_{002} = 9.888$ Å) schist near Alp Sponda on Pizzo Forno (collector: J. B. Thompson, Jr.), we have observed in thin section a selvage of sillimanite needles, coarser than those in α39, adjacent to unbent kyanite. This occurrence is in the same area where Keller (1968, p. 41–47) found kyanite and andalusite in lenses ("Knauer") in textural relationships that suggest that the latter recrystallized from the former. He called on a falling P and T path at a T below that of the triple point to explain the sequential relationship. Other possibilities at Pizzo Forno are that the *P-T* path passed out of the kyanite field into the sillimanite field and then into the andalusite field and that the good expression of these later phases is a consequence of rapid unloading with a broad loop in the *P-T* path extending to considerably higher temperatures than those of α39. Given the negative dP/dT of the andalusite-sillimanite reaction boundary, a larger *P-T* loop would give a higher T of entry into the andalusite field, thereby facilitating the crystallization of that mineral. Presumably specimen α39 also passed through the andalusite field, but at too low a temperature for reaction in the available time.

References

ADAMS, H. G. (1971) *Solid Inclusion Piezothermometry: Experimental Calibration of Quartz-Almandine and Sillimanite-Almandine*. Ph.D. Dissertation, University of California, Los Angeles, 156 p.

——, L. H. COHEN, AND J. L. ROSENFELD (1970) Solid inclusion piezothermometry: Experimental calibration of quartz-almandine and sillimanite-almandine. *Geol. Soc. Am. Abstr. Programs*, **2**, 479.

——, ——, AND —— (1975) Solid inclusion piezothermometry. I: Comparison dilatometry. *Am. Mineral*, **60**, 574–583.

BEVINGTON, P. R. (1969) *Data Reduction and Error Analysis for the Physical Sciences*. McGraw-Hill, Inc., New York, 336 p.

CARSTENS, HARALD (1971) Plastic stress relaxation around solid inclusions in pyrope. *Contrib. Mineral. Petrol.* **32**, 289–294.

CLARK, S. P., JR., AND E. JÄGER (1969) Denudation rate in the Alps from geochronologic and heat flow data. *Am. J. Sci.* **267**, 1143–1160.

CLAYTON, R. N., J. R. O'NEILL, AND T. K. MAYEDA (1972) Oxygen isotope exchange between quartz and water. *J. Geophys. Res.* **77**, 3057–3067.

COHEN, L. H., WILLIAM KLEMENT, JR., AND H. G. ADAMS (1974) Yet more observations on the high-low quartz inversion: Thermal analysis studies to 7 kbar with single crystals. *Am. Mineral.* **59**, 1099–1104.

FREY, MARTIN (1969) Die Metamorphose des Keupers vom Tafeljura bis zum Lukmanier-Gebiet. *Beitr. Geol. Karte Schweiz, Neue Folge*, 137 *Lieferung*, Schweiz. Geologischen Kommission, Bern, 160 p.

GARLICK, G. D., AND S. EPSTEIN (1967) Oxygen isotope ratios in coexisting minerals of regionally metamorphosed rocks. *Geochim. Cosmochim. Acta*, **31**, 181–214.

GOLDSMITH, J. R., AND R. C. NEWTON (1969) *P-T-X* relations in the system $CaCO_3$–$MgCO_3$ at high temperatures and pressures. *Am. J. Sci.* **267-A**, 160-190.

HOLDAWAY, M. J. (1971) Stability of andalusite and the aluminum silicate phase diagram. *Am. J. Sci.* **271**, 97–131.

KELLER, FRANZ (1968) Mineralparagenesen und Geologie der Campo Tencia—Pizzo Forno-Gebirgsgruppe. *Beitr. Geol. Karte Schweiz, Neue Folge*, 135 *Lieferung*, Schweiz. Geologischen Kommission, Bern, 71 p.

KLEMENT, W., JR., AND L. H. COHEN (1968) High-low quartz inversion: Thermodynamics of the transition. *J. Geophys. Res.* **73**, 2249–2259.

LAHEE, F. H. (1941) *Field Geology*, 4th ed. McGraw-Hill, Inc., New York and London, 853 p.

NADAI, A. (1950) *Theory of Flow and Fracture of Solids*, Vol. One, 2nd ed. McGraw-Hill Book Co., Inc., New York, 572 p.

NEWTON, R. C. (1966) Kyanite-andalusite equilibrium from 700° to 800°C. *Science*, **153**, 170–172.

NIGGLI, E. (1970) Alpine metamorphose und alpine gebirgsbildung. *Fortschr. Mineral.* **47**, 16–26.

NYE, J. F. (1957) *Physical Properties of Crystals*. Oxford Univ. Press, London, 322 p.

RICHARDSON, S. W., M. C. GILBERT, AND P. M. BELL (1969) Experimental determination of kyanite-andalusite and andalusite-sillimanite equilibria: the aluminum silicate triple point. *Am. J. Sci.* **267**, 259–272.

ROSENFELD, J. L. (1969) Stress effects around quartz inclusions in almandine and the piezothermometry of coexisting aluminum silicates. *Am. J. Sci.* **267**, 317–351.

——, AND A. B. CHASE (1961) Pressure and temperature of crystallization from elastic effects around solid inclusions in minerals. *Am. J. Sci.* **259**, 519–541.

——, J. B. THOMPSON, AND E-AN ZEN (1958) Data on coexistent muscovite and paragonite. *Geol. Soc. Am. Bull.* **69**, 1637.

SKINNER, B. J. (1956) Physical properties of end-members of the garnet group. *Am. Mineral.* **41**, 428–436.

SOGA, NAOHIRO (1967) Elastic constants of garnet under pressure and temperature. *J. Geophys. Res.* **72**, 4227–4234.

STEIGER, R. H. (1964) Dating of orogenic phases in the central Alps by K-Ar ages of hornblende. *J. Geophys. Res.* **69**, 5407–5421.

THOMPSON, J. B., JR., AND S. A. NORTON (1968) Paleozoic regional metamorphism in New England and adjacent areas. In E-an Zen, W. S. White, J. B. Hadley, and J. B. Thompson, Jr., Eds., *Studies of Appalachian Geology: Northern and Maritime*. New York, Wiley, Interscience Publishers, p. 319–327.

VERMA, R. K. (1960) Elasticity of some high-density crystals. *J. Geophys. Res.* **65**, 757–766.